Experimental and Theoretical Study of the p- and n-Doped States of Alkylsulfanyl Octithiophenes

Carlo Bruno,[†] Francesco Paolucci,[†] Massimo Marcaccio,*[,†] Rois Benassi,[‡] Claudio Fontanesi,*[,‡] Adele Mucci,[‡] Francesca Parenti,[‡] Lisa Preti,[‡] Luisa Schenetti,[‡] and Davide Vanossi[‡]

Dipartimento di Chimica "G. Ciamician", Università di Bologna, via Selmi 2, 40126 Bologna, Italy and Dipartimento di Chimica, Università di Modena e Reggio Emilia, via Campi 183, 41100 Modena, Italy

Received: December 30, 2009; Revised Manuscript Received: May 11, 2010

The charge-transfer and spectral properties of two octithiophenes, namely 4′,4‴,3′ᵛ,3ᵛ′-tetra(octylsulfanyl)-2,2′:5′,2″:5″,2‴:5‴,2′ᵛ:5′ᵛ,2ᵛ:5ᵛ,2ᵛ′:5ᵛ′,2ᵛ″-octithiophene and 4,3″,4ᵛ,4ᵛ″-tetrabromo-4′,4‴,3′ᵛ,3ᵛ′-tetra[(R)-2-methylbutylsulfanyl]-2,2′:5′,2″:5″,2‴:5‴,2′ᵛ:5′ᵛ,2ᵛ:5ᵛ,2ᵛ′:5ᵛ′,2ᵛ″-octithiophene, **OT1** and **OT2**, respectively, are characterized by cyclic voltammetry and spectroelectrochemistry under ultradry conditions. The analysis of the voltammetric results shows the formation of up to the dication for both **OT1** and **OT2** and up to the tetraanion (**OT1**) and trianion (**OT2**) anions. The optical properties of the **OT1** (2+, 1+, neutral, 1−, 2−) species were probed by in situ UV−vis-NIR spectroelectrochemistry. The calculated standard potentials at the B3LYP/cc-pVTZ level of the theory allowed the rationalization of the experimental electrochemical results. The UV−vis-NIR spectra were successfully compared with the theoretical electronic transitions and oscillator strength data obtained by time-dependent B3LYP/6-31G* calculations. Theoretical redox potentials and optical transitions properties are calculated including "the solvent effect" within the CPCM model. The consistency obtained between experimental and theoretical results indicates the existence of the hypothesized high-spin/high-charge p- and n-doped electronic states for the **OT1** and **OT2** octithiophenes here studied.

Introduction

Polythiophenes are an extremely interesting class of compounds from both the scientific and applicative point of view, still at present being an extensively studied subject. This interest is further witnessed by a number of reviews relevant to the most different aspects concerning polythiophenes properties, focusing on more generic and synthetic aspects,[1,2] electrochemically based synthetic routes and electronic properties,[3,4] and possible application as chemical sensors.[5]

Of particular interest appears the possible application of polythiophenes in semiconductors developed within the so-called "bulk heterojunction (BHJ)" approach.[6] The latter is based on blending donor and acceptor materials, thus yielding a large donor−acceptor interfacial area achieved through controlling the phase separation between the two components in bulk. In this way, any absorbing site in the composite is within a few nanometers of the donor−acceptor interface, where the formation of a bicontinuous network creates two channels to transport holes in the donor domain and electrons in the acceptor domain, resulting in efficient charge collection.

In fact, polythiophene represents the most important conjugated polymer utilized in a broad spectrum of applications such as conducting polymers, light-emitting diodes, field-effect transistors, and plastic solar cells due to its excellent optical and electrical properties as well as exceptional thermal and chemical stability.[7] Of course, the rationalization of the interplay between molecular structure and electronic properties is of uttermost importance to achieve the ability to design molecular architectures showing suitable electronic properties. Within this framework, two tiophene-based oligomers, 4′,4‴,3′ᵛ,3ᵛ′-tetra(octylsulfanyl)-,2′:5′,2″:5″,2‴:5‴,2′ᵛ:5′ᵛ,2ᵛ:5ᵛ,2ᵛ′:5ᵛ′,2ᵛ″-octithiophene **OT1** and 4,3″,4ᵛ,4ᵛ″-tetrabromo-4′,4‴,3′ᵛ,3ᵛ′-tetra[(*R*)-2-methylbutylsulfanyl]-2,2′:5′,2″:5″,2‴:5‴,2′ᵛ:5′ᵛ,2ᵛ:5ᵛ,2ᵛ′:5ᵛ′,2ᵛ″-octithiophene **OT2** (Chart 1) are herein considered. Although structurally both **OT1** and **OT2** show the same regiochemistry, **OT1** features four-sided eight-carbon linear alkyl chains whereas in **OT2** four bromines are bound to the polythiophene backbone as well as four-sided five-carbon branched alkyl chains. In particular, in this paper the n-doped (reduced species) and p-doped (oxidized species) states are

CHART 1

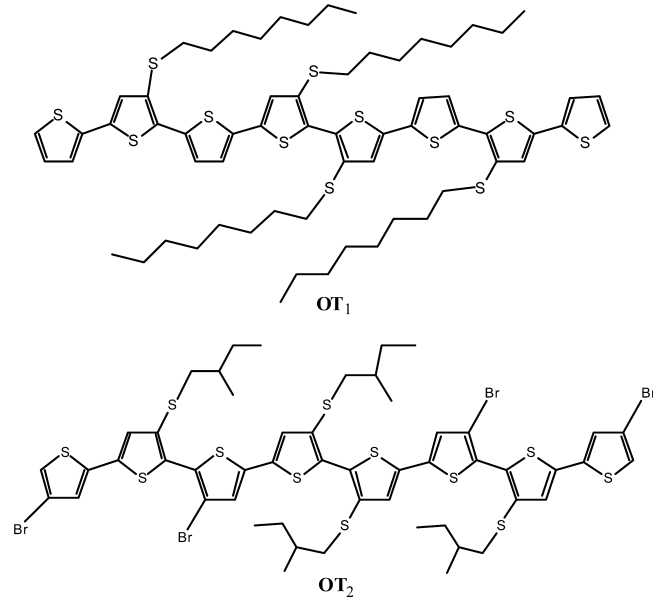

* To whom correspondence should be addressed. E-mail: (C.F.) claudio.fontanesi@unimore.it; (M.M.) massimo.marcaccio@unibo.it.
† Università di Bologna.
‡ Università di Modena e Reggio Emilia.

10.1021/jp9122612
Published on Web 06/16/2010

characterized by using cyclic voltammetry (CV) measurements in ultradry and strictly aprotic environment, in situ UV−vis-NIR spectroelectrochemical experiments and DFT ab initio calculations.

Experimental Section

OT1 and **OT2** were synthesized starting from 4-(octylsulfanyl)-2,2′-bithiophene, 4-bromo-4′-[(S)-2-methylbutylsulfanyl]-2,2′-bithiophene by one-pot oxidative coupling with $FeCl_3$.[8] The chain length of the obtained oligomers was derived from the mass spectra and the regiochemistry from 1D and 2D NMR spectra.

Electrochemical Measurements. Tetrabutylammonium hexafluorophosphate (TBAH, electrochemical grade from Fluka) was used as received as supporting electrolyte. Dichloromethane (DCM), acetonitrile (ACN), and tetrahydrofuran (THF) were purified and dried as previously reported,[9] stored in a specially designed Schlenk flask, and protected from light.

All the solvents were distilled via a closed system into an electrochemical cell, containing the supporting electrolyte and the species under examination, immediately before performing the experiment. Electrochemical experiments were carried out in an airtight single-compartment cell described elsewhere,[9] using platinum as working and counter electrodes and a silver spiral as a quasi-reference electrode. The drift of the quasi-reference electrode was negligible during the time required for an experiment. All the $E_{1/2}$ potentials were directly obtained from cyclic voltammetric curves as averages of the cathodic and anodic peak potentials and by digital simulation for those processes, which are not Nernstian, or for processes closely spaced in multielectron voltammetric peaks. The $E_{1/2}$ values, referenced to the saturated calomel electrode (SCE), were determined by adding ferrocene at the end of each experiment as an internal standard and measuring them with respect to the ferrocinium/ferrocene couple standard potential. The temperature-dependent ferrocinium/ferrocene couple standard potential was measured with respect to SCE by a nonisothermal arrangement according to the method outlined by Weaver et al.[10]

The cell containing the supporting electrolyte and the electroactive compound was dried under vacuum at 100−120 °C for at least 60 h before each experiment. The pressure measured in the electrochemical cell prior to performing the trap-to-trap distillation of the solvent was typically $1-2 \times 10^{-5}$ mbar. Voltammograms were recorded with an AMEL Mod. 552 potentiostat or a custom-made fast potentiostat[11] controlled by an AMEL Mod. 568 programmable function generator. The potentiostat was interfaced to a Nicolet Mod. 3091 digital oscilloscope and the data transferred to a personal computer by the program Antigona.[12] Minimization of the uncompensated resistance effect in the voltammetric measurements was achieved by the positive-feedback circuit of the potentiostat. Digital simulations of the cyclic voltammetric curves were carried out either by Antigona or DigiSim 3.0. The determination of the potentials, for the irreversible processes, was obtained by digital simulation of the cyclic voltammetric curves[13] utilizing a best fitting procedure of the experimental curves recorded at different scan rates spanning over, at least, 2 orders of magnitude.

UV−vis-NIR absorption spectroscopy and Spectroelectrochemistry. UV−vis-NIR absorption spectra were recorded on a Varian spectrophotometer (CARY5). The spectroelectrochemical experiments were carried out using a quartz OTTLE cell with a 0.03 cm pathlength. Temperature control was achieved by a special homemade cell holder with quartz windows in which two nitrogen fluxes (one at room temperature and the other at low temperature) are regulated by two needle valves. All the spectra were recorded by a Cary 5. All the experimental details for the spectroelectrochemical setup were reported elsewhere.[14]

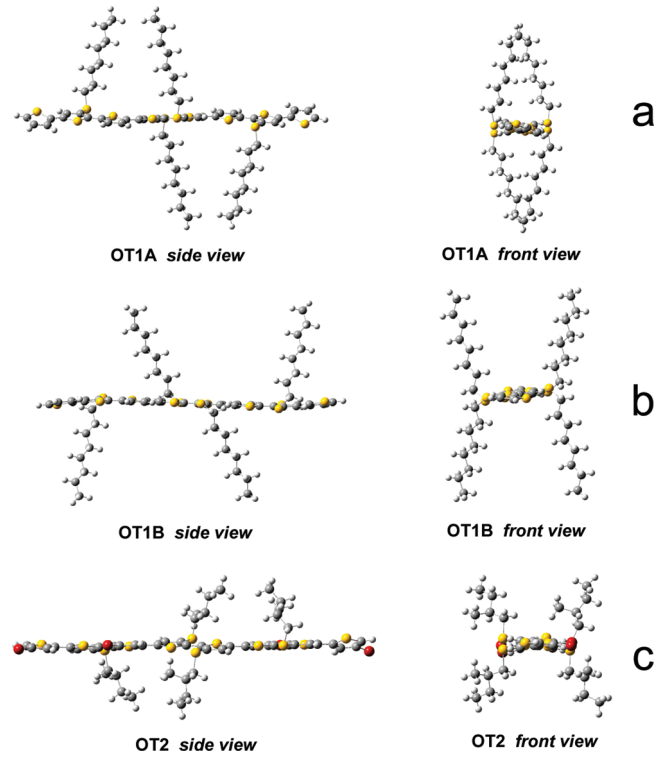

Figure 1. Molecular structures and conformers of the (a,b) **OT1** and (c) **OT2** oligomers.

Computational Details. Ab initio molecular orbital calculations were performed using the Gaussian 03[15] and Firefly QC package[16] suite of programs, the latter is partially based on the GAMESS (U.S.)[17] source code. Great attention and a large endeavor was devoted to a detailed conformational analysis due to the large number of conformational degrees of freedom typical of the compounds here studied. Screening full optimization geometry calculations, aiming to compare B3LYP/3-21G* and B3LYP/6-31G* results, were performed in the vacuum without symmetry constraint in the case of the neutral **OT1** species only. A variety of reasonable starting "guess" conformations have been probed, that is, various thiophene ring and side alkyl chain reciprocal orientations. A complete qualitative agreement is found between the two levels of the theory, and the main features can be summarized as follows: (i) the eight ring framework is found always laying in a planar conformation (thus allowing for the maximum optimization of electronic conjugation of aromatic/π electrons), (ii) the lateral chains are found in a "coil-like" conformation, as shown in Figure 1a. An alternative conformation, which has an energy 3.0 (at B3LYP/3-21G*) and 3.5 (at B3LYP/6-31G*) kcal mol^{-1} higher with respect to the coil-like conformer, is found for which the side alkyl chains appear to maximize their reciprocal distance (Figure 1b). In the following, these two conformations will be referred as "coiled" (**OT1A**) and "unfold" (**OT1B**) species, as shown in Figure 1 panels a and b, respectively. In the case of the **OT2** oligomer, the lowest in energy conformer shows an intermediate structure between **OT1A** and **OT1B** in that the alkyl chains show an arrangement resembling the **OT1A** conformer in the side view and the **OT1B** conformer in the front view, Figure 1c. At variance of **OT1**, the conformational analysis for **OT2** yielded only one structure definitively lower in energy; all of the other conformers optimized were characterized by higher

energies (at least 25 kcal mol^{-1}). Thus, full geometry optimization, always without symmetry constraints, was performed at the B3LYP/3-21G* level of the theory for the **OT1A**, **OT1B**, and **OT2** species here studied (closed and open shell). Geometries optimized in the gas phase were used to perform solvation energy calculation of the various species involved in the determination of the redox potential, by using the Barone and Cossi's polarizable conductor model (CPCM) method,[18] which is based on the polarized continuum model (PCM) of Tomasi.[19] Thus, the ionization potential (IP) and electron affinity (EA) values, relevant to the theoretical calculation of the redox potentials, were determined at the B3LYP/cc-pVTZ//B3LYP/3-21G* level of theory while solvation energies were obtained at the B3LYP/6-31G*//B3LYP/3-21G* level of theory. Note that the variation in the solvent dielectric constant as a function of the temperature has been accounted for by using the suitable experimental values,[20] thus the theoretical redox potentials refer to $T = -70$ °C, while, the "full" thermal contribution (the vibrational frequency calculation is needed) has been neglected because of (i) its negligible quantitative contribution, as evidenced in recent papers,[9a] and (ii) the extremely demanding computational resources needed for the relevant Hessian calculations. Vertical electronic excitation energies were calculated for the **OT1** species (2−, 1−, neutral, 1+, 2+ oxidation states) only, using time-dependent density functional theory (TD-DFT) at the B3LYP/6-31G(d) level of the theory.

Results and Discussion

Electrochemistry. The redox properties of the two oligothiophenes **OT1** and **OT2** were investigated in various aprotic solvents under strictly dry conditions both in the reduction and oxidation regions. A good solubility of the two species, suitable for electrochemical investigation, was obtained in THF and DCM, where a similar behavior was observed for both species. In the following, only the results obtained in THF will be discussed in detail. The voltammetry of **OT1** in THF, at both room and low temperature (Figure 2), shows four reversible one-electron successive reduction processes. Notably, this is the first case where the formation of highly charged, stable n-doped states of a polythiophene species is observed. Few examples have previously been reported relative to the reduction of oligothiophenes, a process which has been described as a "difficult" one.[21] The first two reduction peaks appear as very closely spaced processes while the last two reductions are well separated peaks. At low temperature (−70 °C), the first two processes are slightly better resolved than at room temperature, and in this condition also two oxidation processes are observed within the rather narrow positive potential window allowed by TBAH/THF. While the two closely spaced one-electron oxidations (whose stoichiometry was determined by chronoamperometric measurements) are still chemically reversible, the heterogeneous electron transfer processes are clearly more sluggish than the corresponding reductions, as confirmed by the digital simulation of the voltammetric curves of about 1 order of magnitude ($k_h = 3 \times 10^{-2}$ cm/s for the reductions and $k_h = 5 \times 10^{-3}$ cm/s for the oxidation processes). Moreover, the oxidations are affected by the rather strong adsorption phenomena, as shown in the reverse scan by the characteristic triangularly shaped peak on the cathodic part of the first oxidation. All potentials $E_{1/2}$, relative to either reduction or oxidation processes are collected in Table 1.

The bromo-oligomer **OT2** shows a strikingly different electrochemical behavior with respect to **OT1**, featuring all irreversible subsequent reduction and oxidation processes. In fact, the first oxidation process is only partially irreversible at −70 °C (Figure 3) while all other processes remained totally irreversible even at scan rate as high as 100 V/s. Such a severe irreversibility of all redox processes is likely to have been attributed to the subsequent following-up dissociation of the C−Br bond, occurring on a relatively shorter time scale than the voltammetric one, and involving the formation of bromide and oligothiophenyl radicals R-Br$_{4-n}$ (with $n = 1, 2, 3$) that, in turn, undergo a chemical reaction to give the species RH$_n$Br$_{4-n}$ (with $n = 1, 2, 3$) (vide infra in the Theoretical Results).[22,23]

The **OT2** potentials $E_{1/2}$ collected in Table 1, for the various redox steps, have been obtained by digital simulation of the CV curves at different scan rates (vide supra). The voltammetric simulation evidenced that the reduction processes are more sluggish than the corresponding reductions of **OT1** by about 2

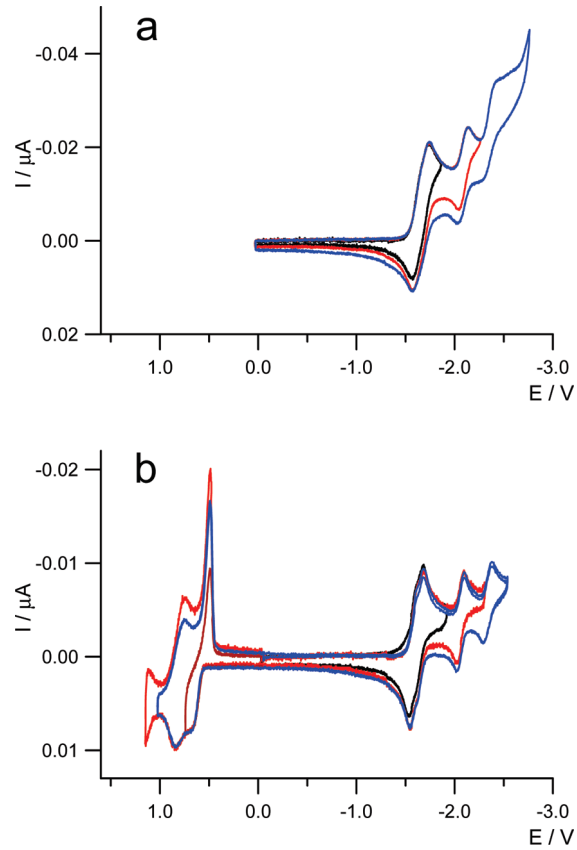

Figure 2. Cyclic voltammetric curves of 1 mM **OT1** solution in 0.07 M TBAH/THF electrolyte at (a) 25 °C and (b) −70 °C; working electrode Pt disk, 125 μm diameter; scan rate 1 V/s; reference electrode SCE.

TABLE 1: Theoretical and Experimental Reduction Standard Potentials in TBAH/THF (vs SCE, at $T = -70$ °C)[a]

	theoretical/V		exp/V	theoretical/V	exp/V
half-reaction	**OT1A**	**OT1B**		**OT2**	
Ox(II)	0.70	0.56	0.79	0.77	1.50
Ox(I)	0.31	0.13	0.59	0.63	1.09
Red(I)	−1.82	−2.09	−1.61	−1.79	−1.40
Red(II)	−2.50	−2.56	−1.70	−2.31	−1.72
Red(III)	−3.04	−3.07	−2.09	−2.70	−2.15
Red(IV)	−3.70	−3.69	−2.36		

[a] The theoretical values are calculated using Scheme 2 at the B3LYP/cc-pVTZ//B3LYP/6-31G* level of theory for the EAs and the IPs and at B3LYP/6-31G*//B3LYP/6-31G* quality for the solvation Gibbs energies.

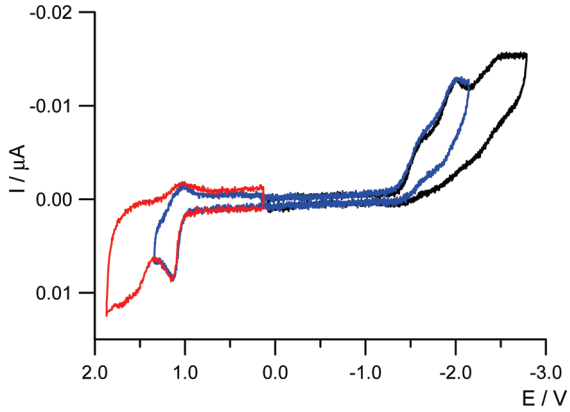

Figure 3. Cyclic voltammetric curves of 1 mM **OT2** solution in 0.07 M TBAH/THF electrolyte at −70 °C; working electrode Pt disk, 125 μm diameter; scan rate 1 V/s; reference electrode SCE.

SCHEME 1

$\mathbf{OT}^{1+} \leftrightarrows \mathbf{OT}^{2+} + e^-$	⇔	IP(II)	⇔	$E_O^0(II)$	⇔	*Ox(II)*
$\mathbf{OT} \leftrightarrows \mathbf{OT}^{1+} + e^-$	⇔	IP(I)	⇔	$E_O^0(I)$	⇔	*Ox(I)*
$\mathbf{OT} + e^- \leftrightarrows \mathbf{OT}^{1-}$	⇔	EA(I)	⇔	$E_R^0(I)$	⇔	*Red(I)*
$\mathbf{OT}^{1-} + e^- \leftrightarrows \mathbf{OT}^{2-}$	⇔	EA(II)	⇔	$E_R^0(II)$	⇔	*Red(II)*
$\mathbf{OT}^{2-} + e^- \leftrightarrows \mathbf{OT}^{3-}$	⇔	EA(III)	⇔	$E_R^0(III)$	⇔	*Red(III)*
$\mathbf{OT}^{3-} + e^- \leftrightarrows \mathbf{OT}^{4-}$	⇔	EA(IV)	⇔	$E_R^0(IV)$	⇔	*Red(IV)*

SCHEME 2: Thermodynamic Cycle for the Calculation of the Redox Potentials[a]

$$\begin{array}{ccc} \mathbf{OT}^{n}_{(g)} + e^- & \xrightarrow[\Delta G(I)^0]{} & \mathbf{OT}^{n-1}_{(g)} \\ \downarrow \Delta G(II)^0_{(solv)} & & \downarrow \Delta G(III)^0_{(solv)} \\ \mathbf{OT}^{n}_{(solv)} + e^- & \xrightarrow[\Delta G(IV)^0]{} & \mathbf{OT}^{n-1}_{(solv)} \quad (3) \end{array}$$

$$1/2\ H_{2(aq)} \xrightarrow[\Delta G^0_{(H)}]{} H^+_{(aq)} + e^- \quad (4)$$

$\Delta G^0_{(H)} = 4.44$ eV[25]

[a] $n = 2+, 1+, 0, 1-, 2-, 3-$ for the half-reactions of Scheme 1 from Ox(II) to Red(IV).

orders of magnitudes ($k_h = 4 \times 10^{-4}$ cm/s), confirming a qualitative comparison analysis of the experimental curves.

Theoretical Results. The redox processes underlying the electrochemical behavior of the octithiophenes here investigated are considered as successive reversible single-step electronic processes. The electrochemical reactivity can be summarized in the Scheme 1 where **OT** stands for the two conformers **OT1A** and **OT1B** (see Figure 1) while, in the case of **OT2**, the redox half-reaction Red(IV) has to be disregarded.

The calculation of the standard potential can be pursued by using the Nernst equation. The standard Gibbs energy, $\Delta G^\circ = -FE^\circ$, relevant to each redox process, is determined exploiting a thermodynamic cycle (Scheme 1), as proposed by Cramer and Truhlar,[24] where $n = 2+, 1+, 0, 1-, 2-, 3-$ ($3-$ only for the **OT1A** and **OT1B** species). The gas-phase Gibbs energies of both reactants and products, as well as the relevant solvation energy, are the quantities involved in the calculation of the redox potential. The standard reduction potential of the $\mathbf{OT}^n/\mathbf{OT}^{n-1}$ couple in solution is calculated as the sum of individual contributions (Scheme 2). The Gibbs energy variation of the whole reduction process is the sum of the two contributions due to the $\mathbf{OT}^n/\mathbf{OT}^{n-1}$ couple and hydrogen reduction half-reactions; thus, $\Delta G^\circ_{red}(\mathbf{OT}^n/\mathbf{OT}^{n-1}$ vs NHE$) = \Delta G^\circ_{red}$(IV) $+ \Delta G^\circ_{ox}$. In Scheme 2, step IV represents the half-reaction Gibbs energy variation of the reduction process in solution, ΔG°_{red}(IV) $= \Delta G^\circ_{red}$(I) $+ \Delta G^\circ_s$(III) $- \Delta G^\circ_s$(II), where ΔG°_{red}(I) = EA $+ \Delta G^\circ_{evr,gas}$ and the $\Delta G^\circ_{evr,gas}$ (with reference to the $\mathbf{OT}^n_{gas} + e^- \rightarrow \mathbf{OT}^{n-1}_{gas}$ reaction) term reflects the difference in thermal contributions to the Gibbs energy of **OT** due to changes in the electronic, vibrational, and rotational partition functions upon reduction. Note that, in the present paper the contribution of the $\Delta G^\circ_{evr,gas}$ has been neglected, this owing both to the prohibitive run time needed for the relevant Hessian calculations and to its negligible contribution as already observed in the literature.[9a,24]

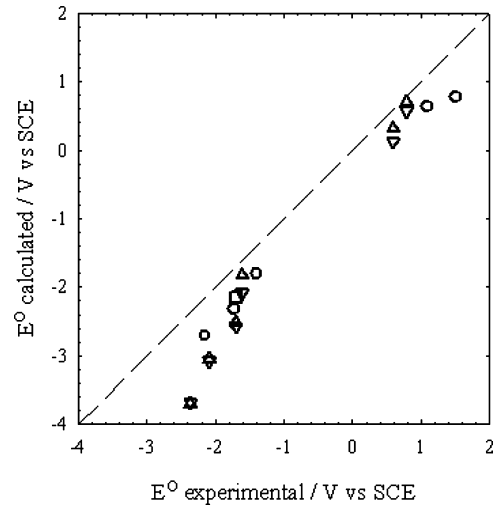

Figure 4. Theoretical versus experimental potentials. The symbols meaning are as follows: **OT1A** (△), **OT2** (○), **OT1B** (▽). The unique point relative to **OT1** (□) concerns the half reaction Red(II) of Scheme 1.

The ΔG°_s(III) and ΔG°_s(II) are the solvation Gibbs energies of the reduced and oxidized species respectively, the two lateral branches of Scheme 2.

Table 1 sets out the calculated and experimental standard potentials, the theoretical values are listed in three columns, which are relative to the **OT1A**, **OT1B**, and **OT2** species (**OT1A** and **OT1B** data are relevant to the coiled and unfold conformations, as described above in Computational Details). Theoretical data reported in Table 1 are obtained at the B3LYP/cc-pVTZ//B3LYP/3-21G* level of the theory concerning the calculation of EAs and IPs; solvation Gibbs energies are of B3LYP/6-31G*//B3LYP/3-21G* quality (the gas phase optimized geometry were used, following the Cramer and Truhlar approach).

Figure 4 shows the theoretical versus experimental standard potentials data, resulting in a rather satisfactory pattern. In particular, the four different symbols refer to the redox processes concerning the **OT1A** (△), **OT1B** (▽), **OT2** (○) species. The unique (□) point concerns the **OT1** half reaction Red(II), where the theoretical E^0_R(I) value is reckoned assuming that a change in conformation, from the coiled (oxidated form) to the unfold (reduced form), occurs. This can be represented by the half-reaction $\mathbf{OT1A}^{1-} + e^- \leftrightarrows \mathbf{OT1B}^{2-}$, and the relation (see Scheme 1) EA $= E_{\text{total electronic energy}}(\mathbf{OT1B}^{2-}) - E_{\text{total electronic energy}}(\mathbf{OT1A}^{1-})$, which holds for the species $\mathbf{OT1B}^{2-}$ and $\mathbf{OT1A}^{1-}$; the quantities $\Delta G(II)^0_{(solv)}$ and $\Delta G(III)^0_{(solv)}$ are calculated for the $\mathbf{OT1A}^{1-}$ and $\mathbf{OT1B}^{1-}$ species respectively.

Note that, the calculated versus experimental least-squares fitting can be accounted twice, because the **OT1A** and **OT1B**

results can be independently considered; that is, considering the **OT1A** (△) and **OT2** (○) set of data or the **OT1B** (▽) and **OT2** (○) set of data, which eventually yields (i) $E^0_{theo} = -0.49 + 1.12\ E^0_{exp}$, $r^2 = 0.96$ for the **OT1A** and **OT2** set, (ii) $E^0_{theo} = -0.55 + 1.11\ E^0_{exp}$, $r^2 = 0.97$ for the **OT1B** and **OT2** set. Remarkably, the slope of the least-squares fit is quite close to unity, as expected in the case of an electronic charge transfer occurring at the electrode/solution interface (under the potential difference of about 1 V[26]). Nonetheless, a closer inspection of the data shows, in some cases, a not negligible difference between theoretical and experimental values, the latter ranging between 0.09 V (the best result) for the $\mathbf{OT1A}^{1+} \leftrightarrows \mathbf{OT1A}^{2+} + e$ process and 1.34 V (the worst result) for the $\mathbf{OT1A}^{3-} + e \leftrightarrows \mathbf{OT1A}^{4-}$ process.

It is worth noting that in the literature a closer quantitative agreement between experimental and theoretical potentials involving the formation of multi charged species (in fact, up to the formation of a trianion) was found, even at a lower level of the theory.[9a,24,27]

In fact, a loose relation can be found between the magnitude of the error and the absolute value of the oxidation state of the specie involved in the redox reaction, that is, larger errors are found when the **OT2** dication and **OT1** tetra-anion are considered. The deviation from theoretical and experimental potentials can stem from different reasons, which could be related to (i) an inadequate level of the theory when dealing with the calculation of electronic properties, (ii) conformational inconsistencies (i.e., the use of wrong geometries for the compounds involved in the redox preocess),[28] (iii) the calculation of the solvation Gibbs energy, and (iv) the lack of some fundamental aspects that are not present in the model approach (e.g, the need to include the solvent when dealing with successive redox processes).[27] In the present work the IP and EA values are calculated at the B3LYP/cc-pVTZ level of the theory; the latter combination of basis set and B3LYP functional is found to yield results that in a wide range of molecular systems compares rather well with the experimental ones.[29]

Conformational effects are obviously difficult to treat in the present case, due to the extremely large number of degrees of freedom of **OT1** and **OT2**. For this reason a number of different guess starting conformations has been considered. In particular, concerning the half-reactions Red(III) and Red(IV), where various out-of-plane ring structures, and also a conformer featuring lateral alkyl chains coplanar with the eight ring moiety, has been considered. Concerning **OT1,** only two conformations close in energy were found (**OT1A** and **OT1B**, see the computation details section) and systematically used in the calculations. Nonetheless, both **OT1A** and **OT1B** leads to quite similar theoretical results, even for the half-reactions Red(III) and Red(IV), as can be found in Table 1, while the effect of a conformation change triggered by the charge transfer process is proposed to occur when considering the **OT1** first reduction step (half-reaction Red(I)) whose experimental potential value is extremely close to the second reduction step, i.e., the half-reaction Red(II) (a 0.09 V difference is found between the two processes in Table 1).

In fact, the theoretical value for the $\mathbf{OT1A}^{1-} + e^- \leftrightarrows \mathbf{OT1B}^{2-}$ half-reaction is $E^0_R(II) = -2.15$ V (point □ in Figure 4), showing a difference of 0.33 V with respect to $E^0_R(I) = -1.82$ V (**OT1A** conformer); a result which is dramatically better than the $E^0_R(I) - E^0_R(II)$ difference, in Table 1, found to be 0.68 and 0.47 V for **OT1A** and **OT1B,** respectively. This proposed conformational change, induced by the charge transfer process, will be also assessed on the basis of UV−vis-NIR spectra.[28]

Focusing the attention on possible problems inherent to the calculation of solvation quantities, CPCM B3LYP/6-31G*//B3LYP/3-21G* solvation energies appears to be a solid well grounded level of the theory, even though most of the literature deals with the comparison of experimental and theoretical values concerning neutral species. In fact, theoretical solvation energies calculated within the continuum dielectric solvation model, even though implemented within the highly sophisticated polarizable conductor model (CPCM) method, were already considered to yield underestimated values when dealing with molecular species bearing a net charge.[30] In our case, a [−20 × (anion net charge)] kcal·mol^{-1} contribution[31] is needed to obtain virtually exact standard potential values, in agreement with the results found in the ref 30.

However, a detailed analysis of the **OT1** and **OT2** patterns in Figure 4, suggests that the larger deviations observed between theoretical and experimental values, in particular those concerning **OT1** half-reactions Red(III) and Red(IV) (i.e., the reductions involving high-spin 2−, 3−, and 4− species), could also stem from the calculation of the solvation energy. Note that for half-reactions Red(III) and Red(IV) the difference between theoretical and experimental values are about 1.0 and 1.3 V in the case of **OT1.** This difference reduces to be about 0.5 V for half-reactions Red(III) of **OT2,** although the presence of the high atomic number bromine atoms, in principle, should affect the calculation of electronic properties with larger errors. Such a pronounced difference in the results could come from the structural difference between **OT1** and **OT2**, as the longer lateral alkyl chains in **OT1** could be much more difficult to be modeled by the solvation algorithm, based on a "continuum dielectric" approach, which in general works "better" when dealing with isotropic molecular systems.[32]

A final interesting consideration regards the **OT2** electrochemical behavior upon reduction, where subsequent one-electron processes are observed up to the third reduction, with the probable dissociation of the C−Br bond. Note that the theoretical reduction potentials, reported in Table 1, refer to the **OT2** species, as represented in Scheme 1 (vide supra). However, theoretical potentials were also calculated assuming one-electron dissociative electrochemical reductions, which concerns the four possible consecutive dehalogenations comprising the electron uptake (with the eventual radical anion formation) and the following-up carbon−bromine dissociation, sketched by the reaction $R\text{-}Br_4 \rightarrow R\text{-}Br_{4-n}^{\bullet} + Br^-$ (where n = 1, 2, 3, 4 and the $R\text{-}Br_4$ species represents **OT2**). The four possible steps, leading to the progressive dehalogenation of **OT2** (Figure S1 in the Supporting Information), is in juxtaposition to the model approach reported in Scheme 1, where the formation of an open shell high spin $\mathbf{OT2}^{3-}$ species would be proposed. The theoretical potentials thus calculated do not fit the linear pattern shown in Figure 4. Moreover, the Hessian analysis of the $\mathbf{OT2}^{3-}$, calculated at the B3LYP/6-31G* level of the theory, yielded only positive frequencies, indicating the C−Br bond stability of the $\mathbf{OT2}^{3-}$ species. Eventually, the C−Br bond length is found to increase in the $\mathbf{OT2}^{2+}$, $\mathbf{OT2}^{1+}$, $\mathbf{OT2}^{0}$, $\mathbf{OT2}^{1-}$, $\mathbf{OT2}^{2-}$, $\mathbf{OT2}^{3-}$ series. The debromination mechanism of the species **OT2** upon subsequent reductions is also supported by the calculated redox potentials for the various product species RH_nBr_{4-n} (n = 1, 2, 3) obtained, reported in Table S1 (Supporting Information), which become stepwisely more negative.

Spectroelectrochemistry and TD-DFT Calculations. Since a prerequisite for carrying out spectroelectrochemical investigations is the stability of the charged species produced by the

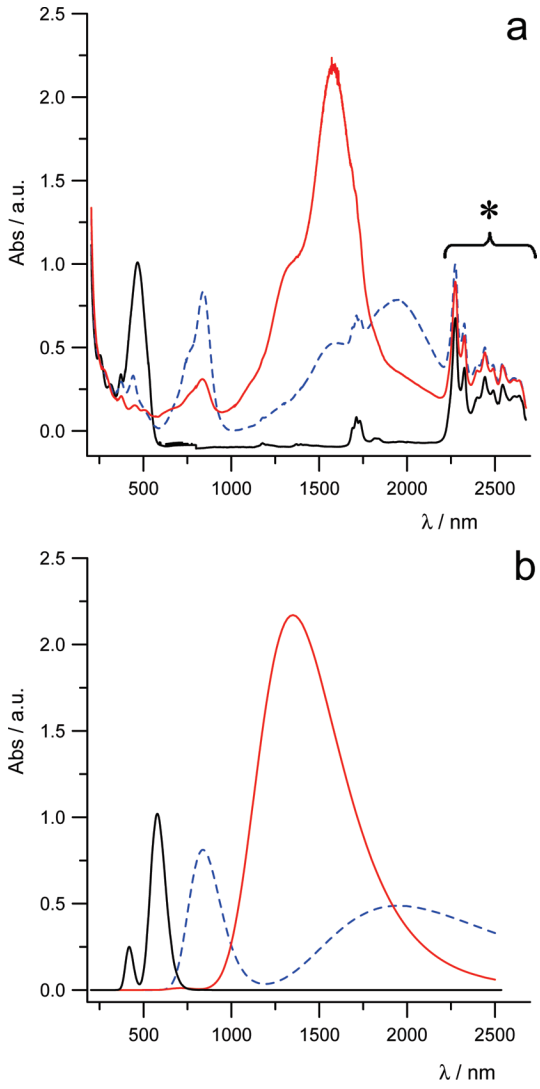

Figure 5. (a) Experimental UV−vis-NIR absorption spectra of the pristine (solid black trace), first reduced state (dashed blue trace), and second reduced state (solid red trace) **OT1** species in TBAH/THF electrolyte solution, $T = -70$ °C in an OTTLE cell; (b) TD-DFT calculated UV−vis-NIR spectra of **OT1** species at its pristine, first and second reduced state. Note that the bands in the NIR region of the experimental spectra (i.e., at about 2200−2600 nm), labeled by the asterisk (*), are due to the electrolyte/solvent.

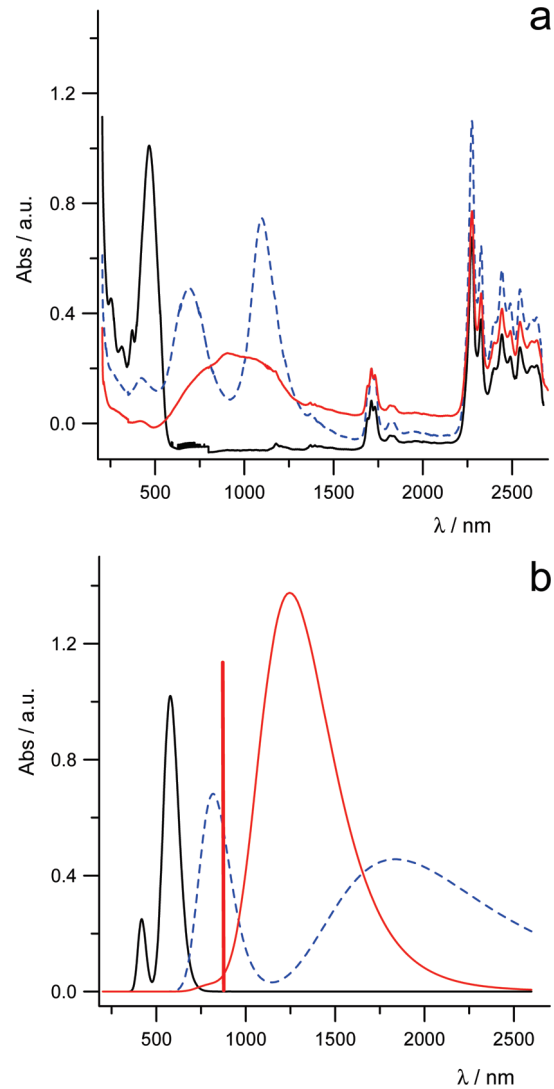

Figure 6. (a) Experimental UV−vis-NIR absorption spectra of the pristine (solid black trace), first oxidized state (dashed blue trace), and second oxidized state (solid red trace) **OT1** species in TBAH/THF electrolyte solution, $T = -70$ °C in an OTTLE cell; (b) TD-DFT calculated UV−vis-NIR spectra of **OT1** species at its pristine, first, and second oxidized state. The red vertical bar at 860 nm represents the theoretical transition of the $\mathbf{OT1}^{2+}$ calculated at SA-MCSCF CAS(4,4) + XMCQDPT level of theory (Table S4 in Supporting Information); the height of the bar is normalized to the oscillator strength. The bands in the NIR region of the experimental spectra (i.e., at about 2200−2600 nm) are due to the electrolyte/solvent.

electrochemical process on the relatively longer time scale of such a technique, UV−vis-NIR spectroelectrochemical data are herein reported only for the reduced, n-doped, or oxidized, p-doped, states of **OT1**, namely, $\mathbf{OT1}^{2+}$, $\mathbf{OT1}^{1+}$, $\mathbf{OT1}^{0}$, $\mathbf{OT1}^{1-}$, $\mathbf{OT1}^{2-}$ species, for which, at odds with **OT2**, steady state (i.e., equilibrium) measurement were allowed. Figure 5a shows the spectrum of the **OT1** species together with those of the monoanion $\mathbf{OT1}^{1-}$ and dianion $\mathbf{OT1}^{2-}$ in the range 260−2600 nm. Upon the first reduction, the band at 480 nm, that is, the only transition observed for the pristine species, largely decreases while two new absorption bands, at 840 and 1950 nm, respectively, appear and grow up. The subsequent further reduction to $\mathbf{OT1}^{2-}$ greatly affects all the absorption bands observed at the monoanion level; the band at 480 nm and the newly born band at 1950 nm disappear while the band at 840 nm largely decreases and a strong absorption band at 1570 nm takes their place. Concerning the spectroelectrochemistry of the oxidation processes (Figure 6a), the spectrum of the $\mathbf{OT1}^{+}$ shows a strong bleaching of the absorption at 480 nm and the growth of two new bands at about 700 and 1100 nm. The second oxidation process yields a sort of merging of the two bands of the $\mathbf{OT1}^{+}$ in a rather broad absorption band with a relatively not very intense maximum at 900 nm. As in the case of the second reduction, the second oxidation also induces the complete disappearance of the band at 480 nm. Finally, the interpretation of the spectroelectrochemical UV−vis-NIR results was assessed by comparison with the time-dependent B3LYP/6-31G* calculations.

They were performed for both the coiled (**OT1A**) and unfold (**OT1B**) conformations. As for the calculations of the redox processes, the inclusion of solvent effect proved to be crucial for obtaining a good agreement between experimental and theoretical results, as displayed in Table 2, Figure 5b, and Figure 6b.

Figure 7a shows the MO diagram concerning the HOMO, LUMO, and SOMO energy levels (a similar MO sketch is found

TABLE 2: Spectroscopic experimental and theoretical data[a]

	exp	OT1A				OT1B			
net charge	nm	nm	*f*	transition	CIC[b]	nm	*f*	transition	CIC[b]
2+[c]	900[d]	1245	3.17	HOMO→LUMO	0.75	1080	3.42	HOMO→LUMO	0.56
1+	1100	1835	1.05	HOMO→LUMO	0.89	1509	0.88	HOMO→LUMO	0.92
	700	817	1.56	SOMO→LUMO	0.91	859	1.89	SOMO→LUMO	0.92
Neutral	480	577	2.35	HOMO→LUMO	0.67	624	2.48	HOMO→LUMO	0.66
1−	1950	1950	0.92	SOMO→LUMO	0.89	2172	0.99	SOMO→LUMO	0.87
	840	837	1.52	HOMO→LUMO	0.92	856	1.61	HOMO→LUMO	0.89
2−	1570	1294	2.91	HOMO→LUMO	0.52	1349	3.14	HOMO→LUMO	0.50

[a] Vertical transition energies and oscillator strengths (*f*), calculated at the TD-DFT B3LYP/6-31G* level of the theory, including CPCM solvation ($T = -70$ °C, $\varepsilon = 11.4$). [b] CI coefficient. [c] The theoretical spectroscopic data for the species with charge 2+ have been also calculated at higher level of theory (see Table S4 in the Supporting Information and Figure 6b). [d] Broad band centered at 900 nm.

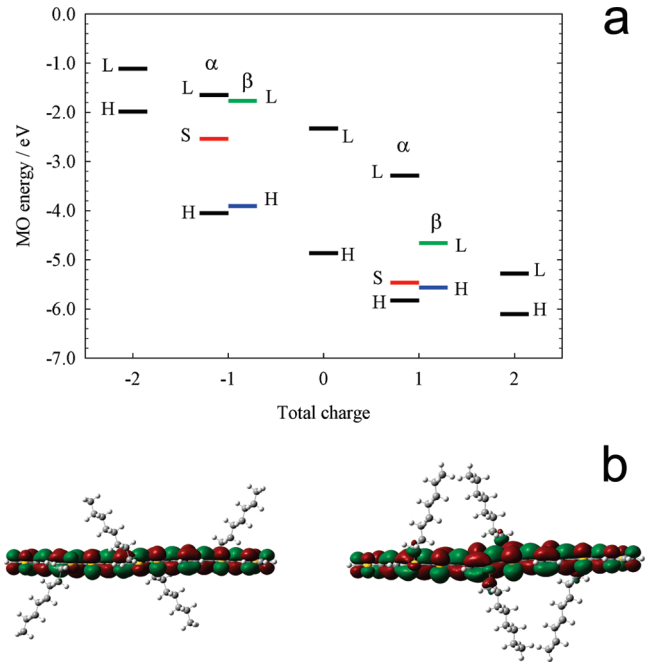

Figure 7. (a) MO energy diagram of **OT1** species at various degrees of oxidation and reduction calculated at B3LYP/6-31G*; (b) HOMO surfaces of **OT1A**$^{2-}$ (right) and **OT1B**$^{2-}$ (left).

for both the **OT1A** and **OT1B** conformers), which accounts for the appearance of one main absorption peak in the 2+, neutral, 2− species, and two peaks in the 1+ and 1− species in the relevant spectra of Figure 5 and Figure 6. Note that, concerning the species with charge 2+ and 2-, the restricted and unrestricted calculations yield the same results and therefore the same MOs pattern (see data in Table S3 in the Supporting Information).

Table 2 shows that the calculated excitation energies for the closed shell species can be assigned to HOMO→LUMO transitions, while, when the open shell species are considered, two strong electronic transitions are predicted. The latter can be assigned to SOMO→LUMO and HOMO→LUMO electronic transitions. In fact, the SOMO→LUMO and HOMO→LUMO difference in energies are similar, Figure 7a, thus accounting for the presence of two main absorption peaks in the experimental spectra, Figure 5 and Figure 6. Note that, in the case of the **OT1** anions, higher energy shoulders are observed associated to each main band (at ∼750 and 1600 nm for the monoanion and at ∼1350 nm for the dianion, Figure 5a) that can be attributed to vibronic coupling, analogously to the reported behavior of the sexythiophene charged species.[33]

It is worth noting that a closer agreement between theoretical and experimental results is found between **OT1A** and experimental data in the case of the monoanion species, while a better agreement is found for the **OT1B** conformer when the dianion species is considered. This further supports the hypothesis of a conformational change accompanying the second reduction process of **OT1**, which is consistent with the discussion concerning the electrochemical behavior. In fact, comparison of the MOs of the **OT1A** and **OT1B**, involved in the electronic transitions, does not show any significant qualitative difference (see, e.g., Figure 7b showing the HOMOs of **OT1A** and **OT1B** dianions). A possible explanation of the lower energy (larger stability) of **OT1B**$^{2-}$ when compared to the **OT1A**$^{2-}$ species has likely to be found in the larger ability of the "open" conformation (**OT1B**) in delocalizing the charge. Thus, the central eight ring thiophene moiety bears a net negative charge of 2.1 electrons (**OT1A**) while **OT1B** is able to accommodate 3.3 electrons allowing for a larger net negative charge separation between the lateral chains and the central eight ring thiophene moiety, that would then bring a more favorable solvation energy in the case of **OT1B**.

Note that for the UV-vis-NIR spectrum of the **OT1**$^{2+}$ species, a not negligible difference is found between the experimental and theoretical absorption maxima, as shown in Table 2 and Figure 6. To elucidate the origin of such discrepancies, excited states calculations have been performed within a wide range of level of theory from semiempirical to multireference model chemistry, aiming to probe also the possible diradical character of the dication species. As a whole, some evidence seem to suggest the inadequacy of DFT-based method to effectively describe the high charge high spin 2+ state. Thus, state-of-the-art SA-MCSCF CAS(4,4) + XMCQDPT calculations have been performed, which give a 860.9 nm vertical transition energy with a 2.93 oscillator strength (vertical bar in Figure 6b). Such a theoretical absorption energy is the unique value that gives the best matching with the experimental result (see and compare all the data in Table S4 of the Supporting Information), despite the agreement between the oscillator strength and the intensity is not so good. However, it is worth noting that some discrepancies might be due to the strong adsorption phenomena occurring in oxidation, as evidenced by the typical triangularly shaped voltammograms (see Figure 2), as well as to the possible electrochemically induced polymerization of **OT1** at higher positive potentials. Experimental evidence indicates that soon after the second oxidation (i.e., at potentials more positive than 1.1 V) a polymeric deposition starts; the subject is currently under investigation and it will be reported in due time.

Conclusions

OT1 and **OT2** show marked differences in their electrochemical behavior, which stem from the structural/electronic influence exerted by the presence of the C_8 linear alkyl chain

versus the bromine/methyl,butyl chain (inducing differences in the conformational analysis).

For the first time, up to four reversible reductive processes are observed and rationalized when dealing with oligothiophens, such as **OT1**, which shows electrochemical reversibility both in the case of the cations (p-doped state) and anions (n-doped state), while the electrochemical behavior of **OT2** upon reduction could be exploited in the functionalization of electrodic surfaces, as the instability, observed in both the electrochemical and spectroelectrochemical measurements, is due to the cleavage of the C−Br bond leading to a octithiophene radical anion and the bromide anion.

Concerning the **OT1** species, it is proposed that a change in conformation from the coiled (oxidated form) to the unfold (reduced form) represented as the half-reaction $\mathbf{OT1A}^{1-} + e^- \leftrightarrows \mathbf{OT1B}^{2-}$, is electrochemically triggered. This view appears supported by the comparison with both spectroelectrochemical and theoretical results.

Acknowledgment. This research was supported by the Italian Ministry of University and Research (MIUR) through the project PRIN 2008, the University of Bologna and University of Modena e Reggio Emilia. INSTM and CINECA are also acknowledged for support and computing facilities.

Supporting Information Available: Optimized molecular structures of partially and completely dehalogenated **OT2** species. Vertical electronic excitation energies and oscillator strength for the **OT1A**, (2− and 2+ redox states), calculated with a large variety of level of the theory ranging from ZINDOS/S + SCI to SA-MCSCF CAS(4,4) + XMCQDPT. This material is available free of charge via the Internet at http://pubs.acs.org.

References and Notes

(1) Schopf, G.; Koβmehl, G. *Adv. Polym. Sci.* **1997**, *129*, 1–166.
(2) McCullough, R. D. *Adv. Mater.* **1998**, *10*, 93–116.
(3) Roncali, J. *Chem. Rev.* **1992**, *92*, 711–738.
(4) Roncali, J. *Chem. Rev.* **1997**, *97*, 173–205.
(5) McQuade, D. T.; Pullen, A. E.; Swager, T. M. *Chem. Rev.* **2000**, *100*, 2537–2574.
(6) Yu, G.; Gao, J.; Hummelen, J. C.; Wudl, F.; Heeger, A. J. *Science* **1995**, *270*, 1789.
(7) Cheng, Y.-J.; Yang, S.-H.; Hsu, C.-S. *Chem. Rev.* **2009**, *109*, 5868.
(8) Mucci, A.; Parenti, F.; Cagnoli, R.; Benassi, R.; Passalacqua, A.; Preti, L.; Schenetti, L. *Macromolecules* **2006**, *39*, 8293–8302.
(9) (a) Bruno, C.; Benassi, R.; Passalacqua, A.; Paolucci, F.; Fontanesi, C.; Marcaccio, M.; Jackson, E. A.; Scott, L. T. *J. Phys. Chem. B* **2009**, *113*, 1954–1962. (b) La Pensée, A. A.; Bickley, J.; Higgins, S. J.; Marcaccio, M.; Paolucci, F.; Roffia, S.; Charnock, J. M. *J. Chem. Soc., Dalton Trans.* **2002**, 4095. (c) Guldi, D. M.; Maggini, M.; Menna, E.; Scorrano, G.; Ceroni, P.; Marcaccio, M.; Paolucci, F.; Roffia, S. *Chem., Eur. J.* **2001**, *7*, 1597–1605.
(10) Yee, E. L.; Cave, R. J.; Guyer, K. L.; Tyma, P. D.; Weaver, M. J. *J. Am. Chem. Soc.* **1979**, *101*, 1131–1137.
(11) Amatore, C.; Lefrou, C. *J. Electroanal. Chem.* **1992**, *324*, 33–58.
(12) Mottier, L. *Antigona*; University of Bologna: Bologna, Italy, 1999.
(13) Spieser, B. In *Electroanalytical Chemistry. A series of Advances*; Bard, A. J., Rubistein, I., Eds.; Marcel Dekker, Inc.: New York, 1996; Vol. 19, p 1 and references therein.
(14) (a) Lee, S.-M.; Marcaccio, M.; McCleverty, J. A.; Ward, M. D. *Chem. Mater.* **1998**, *10*, 3272. (b) Stagni, S.; Palazzi, A.; Zacchini, S.; Ballarin, B.; Bruno, C.; Marcaccio, M.; Paolucci, F.; Monari, M.; Carano, M.; Bard, A. J. *Inorg. Chem.* **2006**, *45*, 695.
(15) Frisch, M. J.; Trucks, G. W.; Schlegel, H. B.; Scuseria, G. E.; Robb, M. A.; Cheeseman, J. R.; Montgomery, Jr., J. A.; Vreven, T.; Kudin, K. N.; Burant, J. C.; Millam, J. M.; Iyengar, S. S.; Tomasi, J.; Barone, V.; Mennucci, B.; Cossi, M.; Scalmani, G.; Rega, N.; Petersson, G. A.; Nakatsuji, H.; Hada, M.; Ehara, M.; Toyota, K.; Fukuda, R.; Hasegawa, J.; Ishida, M.; Nakajima, T.; Honda, Y.; Kitao, O.; Nakai, H.; Klene, M.; Li, X.; Knox, J. E.; Hratchian, H. P.; Cross, J. B.; Bakken, V.; Adamo, C.; Jaramillo, J.; Gomperts, R.; Stratmann, R. E.; Yazyev, O.; Austin, A. J.; Cammi, R.; Pomelli, C.; Ochterski, J. W.; Ayala, P. Y.; Morokuma, K.; Voth, G. A.; Salvador, P.; Dannenberg, J. J.; Zakrzewski, V. G.; Dapprich, S.; Daniels, A. D.; Strain, M. C.; Farkas, O.; Malick, D. K.; Rabuck, A. D.; Raghavachari, K.; Foresman, J. B.; Ortiz, J. V.; Cui, Q.; Baboul, A. G.; Clifford, S.; Cioslowski, J.; Stefanov, B. B.; Liu, G.; Liashenko, A.; Piskorz, P.; Komaromi, I.; Martin, R. L.; Fox, D. J.; Keith, T.; Al-Laham, M. A.; Peng, C. Y.; Nanayakkara, A.; Challacombe, M.; Gill, P. M. W.; Johnson, B.; Chen, W.; Wong, M. W.; Gonzalez, C.; Pople, J. A. *Gaussian 03*, revision C.02; Gaussian, Inc.: Wallingford, CT, 2004.
(16) Granovsky, A. A. *Firefly*, version 7.1.G, 2009; http://classic.chem.msu.su/gran/firefly/index.html.
(17) Schmidt, M. W.; Baldridge, K. K.; Boatz, J. A.; Elbert, S. T.; Gordon, M. S.; Jensen, J. H.; Koseki, S.; Matsunaga, N.; Nguyen, K. A.; Su, S.; Windus, T. L.; Dupuis, M.; Montgomery, J. A. *J. Comput. Chem.* **1993**, *14*, 1347.
(18) Barone, V.; Cossi, M. *J. Phys. Chem. A* **1998**, *102*, 1995.
(19) Miertus, S.; Scrocco, E.; Tomasi, J. *Chem. Phys.* **1981**, *55*, 117.
(20) *Handbook of Chemistry and Physics*, 75th ed.; CRC: Boca Raton, FL, 1994.
(21) (a) Mastragostino, M.; Soddu, L. *Electrochim. Acta* **1990**, *35*, 463. (b) Fahri Alkan, F.; Salzner, U. *J. Phys. Chem. A* **2008**, *112*, 6053–6058.
(22) Since the electrochemical measurements are carried out in a carefully purified and highly aprotic electrolyte solution (see Experimental Section), the reduction of the $C_{aromatic}$-Br containing species is a one-electron process instead of the two-electrons stoichiometry usually observed in the case of added proton donors, as reported in literature (see refs 23e–g).
(23) (a) Benassi, R.; Bertarini, C.; Taddei, F. *Chem. Phys. Lett.* **1996**, *257*, 633. (b) Prasad, M. A.; Sangaranarayanan, M. V. *Chem. Phys. Lett.* **2005**, *414*, 55. (c) Antonello, S.; Maran, F. *Chem. Soc. Rev.* **2005**, *34*, 418. (d) Costentin, C.; Robert, M.; Saveant, J.-M. *Chem. Phys.* **2006**, *324*, 40. (e) Costentin, C.; Robert, M.; Savéant, J.-M. *J. Am. Chem. Soc.* **2004**, *126*, 16051. (f) Costentin, C.; Robert, M.; Savéant, J.-M. *J. Am. Chem. Soc.* **2003**, *125*, 10729. (g) Andrieux, C. P.; Savéant, J.-M.; Tallec, A.; Tardivel, R.; Tardy, C. *J. Am. Chem. Soc.* **1997**, *119*, 2420.
(24) Winget, P.; Weber, E. J.; Cramer, C. J.; Truhlar, D. G. *Phys. Chem. Chem. Phys.* **2000**, *2*, 1231.
(25) Trasatti, S. *Pure Appl. Chem.* **1986**, *58*, 955.
(26) Amatore, C. In *Organic Electrochemistry*, 4th ed.; Lund, H., Hammerich, O., Eds.; Marcel Dekker Inc.: New York, 2001; Chapter 1, pp 1−94.
(27) Fontanesi, C.; Benassi, R.; Giovanardi, R.; Marcaccio, M.; Paolucci, F.; Roffia, S. *J. Mol. Struct.* **2002**, *612*, 277.
(28) Marcaccio, M.; Paolucci, F.; Fontanesi, C.; Fioravanti, G.; Zanarini, S. *Inorg. Chim. Acta* **2007**, *360*, 1154.
(29) (a) Szafran, M.; Koput, J. *J. Mol. Struct.* **2001**, *565−566*, 439–448. (b) Tormena, C. F.; da Silva, G. V. J. *Chem. Phys. Lett.* **2004**, *398*, 466–470.
(30) (a) Holm, A. H.; Brinck, T.; Daasbjerg, K. *J. Am. Chem. Soc.* **2005**, *127*, 2677. (b) Holm, A. H.; Yusta, L.; Carlqvist, P.; Brinck, T.; Daasbjerg, K. *J. Am. Chem. Soc.* **2003**, *125*, 2148.
(31) That is, −20, −40, −60, and −80 kcal mol^{-1} for the mono-, di-, tri- and tetra-anion species, respectively.
(32) (a) Antonello, S.; Benassi, R.; Gavioli, G.; Taddei, F.; Maran, F. *J. Am. Chem. Soc.* **2002**, *124*, 7529–7538. (b) Benassi, R.; Taddei, F. *J. Phys. Chem. A* **1998**, *102*, 6173–6180.
(33) (a) Clarke, T. M.; Gordon, K. C.; Officer, D. L.; Grant, D. K. *J. Phys. Chem. A* **2005**, *109*, 1961–1973. (b) Yokonuma, N.; Furukawa, Y.; Tasumi, M.; Kuroda, M.; Nakayama, J. *Chem. Phys. Lett.* **1996**, *255*, 431–436.

JP9122612